metals

MDPI

Article

The Weldability of Duplex Stainless-Steel in Structural Components to Withstand Corrosive Marine Environments

Iñigo Calderon-Uriszar-Aldaca [1,*], Estibaliz Briz [2], Harkaitz Garcia [2] and Amaia Matanza [3]

[1] TECNALIA, Basque Research and Technology Alliance (BRTA), Mikeletegi Pasealekua 2, 20009 Donostia-San Sebastián, Spain
[2] Department of Mechanical Engineering, University of the Basque Country (UPV/EHU), 48940 Leioa, Vizcaya, Spain; estibaliz.briz@ehu.eus (E.B.); arkaitz.garcia@ehu.eus (H.G.)
[3] SIAME-MPC (UPV/EHU) Université de Pau et des pays de l'Adour ISA BTP, 64600 Anglet, France; a.matanza-corro@univ-pau.fr
* Correspondence: inigo.calderon@tecnalia.com; Tel.: +34-699-907-343

Received: 12 October 2020; Accepted: 3 November 2020; Published: 5 November 2020

Abstract: There is still a considerable gap in the definition of the weldability of Duplex Stainless Steel (DSS). A lack of clarity that is explained by the standard specification of the maximum content of equivalent carbon that defines a "weldable" steel coupled with the fact that the alloying elements of DSS exceed this defined limit of weldability. In this paper, welding quality in an inert environment and in presence of chlorides is analyzed with the aim of defining optimum welding conditions of 2001, 2304, and 2205 DSS. The same procedure is followed for a hybrid weld between DSS 2205 and a low carbon mild steel, S275JR. As main output, this study defined the optimal welding conditions with tungsten inert gas without filler for each type of DSS weld that showed excellent anti-corrosion performance, with the exception of the DSS 2205-S275JR weld where widespread corrosion was observed. Additionally, this study established a relationship between the thermal input during welding and the content of alloying elements in defect-free joints. Furthermore, it demonstrated that an increase in ferrite content did not lead to a worse corrosion resistance, as expected after passivation.

Keywords: stainless steels; weldability; aggressive environments; marine environments; heat input

1. Introduction

Offshore steel structures, but also onshore in coastal areas up to a few km to the coast, suffer the effects of a harsh corrosive marine environment. This is caused mainly by moisture and chlorides that are present in the atmosphere near the sea. Chlorides cause a localized pitting corrosion attack that, in structures under tension, can cause stress concentration hot spots developing the early failure of the structure by sudden crack propagation. Thus, to face this problem, one emerging strategy is the use of Duplex Stainless Steel (DSS) instead of the simply painted carbon steel or other lesser stainless steels. DSS presents better properties, especially in terms of strength, durability, and fire resistance [1,2], when compared to the most widely used carbon structural steel in the construction industry (S275JR). These properties are due to the presence of alloying elements such as nickel and chromium, among others, generating an external protective or passive layer their microstructure, depending on the lower amount of ferrite.

Nevertheless, steel structures are composed by hot-rolled profiles and other singular elements that need to be joined to form them. When these joints are made by welding, the welding itself constitutes a localized thermal treatment that could evaporate the protective elements and change the microstructure, increasing the ferrite fraction. Thus, the protective properties of DSS could be

removed by welding precisely at the more critical spots in joints, that tend to concentrate stresses. Therefore, the research on how to correctly weld these DSS with a proper thermal input is valuable to enable the safe manufacturing of steel structures under marine environment.

The main reason specific building standards, such as the Eurocodes [3–9], have yet to include the use of these steel grades is the uncertainty surrounding spots that are subjected to thermal aggressions. In other words, these standards have not yet included stainless steel in building structures, due to the complexity of establishing the parameters that can guarantee suitable and safe use of the materials after the welding process [10,11].

Consequently, research on the equivalent carbon content method specified in these standards [3–9] indicates that it is well suited to those non-alloyed steels, the so-called weldable steels in the standardization literature. Thus, the application of that method to stainless steel that has a high proportion of alloying elements is pointless, because the equivalent carbon content of them will always exceed the previously set threshold. Weldability as such, therefore, needs to be demonstrated by other alternative methods, which will ensure that the protective properties of the corresponding alloy will be locally retained within the Heat-Affected Zone (HAZ) of the weld.

Locally applied heat treatment, when incorrectly applied, could modify the welding zone of stainless steel, in such a way as to reduce the protective elements of the material and leave residual stresses. For instance, Elsaady et al. presented the behavior of different welding temperature ranges for a duplex steel [12]. The effects on the affected area made it much more vulnerable to corrosive processes such as localized pitting corrosion in a marine environment [13].

However, there is still a key clear gap between current understanding and engineering practice. According to these standards, only "weldable" steels must be used to form steel structures, even more so in marine environments, but only the equivalent carbon content method is prescribed to determine whether a steel is weldable or not, despite it discriminating DSS systematically. Thus, although DSS are in fact weldable under certain conditions and perform much better in marine environments, paradoxically they are unfairly discarded in practice because of not being "weldable" under carbon equivalent content. Therefore, there is still a need for practical and feasible alternative procedures to demonstrate the weldability of a DSS under certain conditions going beyond the equivalent carbon content method.

In fact, there are standardized procedures to see the ferrite content, or the corrosion performance under salt-spray chamber, or to do a visual examination, or to analyze a micrograph looking for intermetallic phases. Every single one of such procedures determines one single property of the DSS welding but is not able individually to determine whether a DSS is weldable or not and, even more importantly, how to do it.

Therefore, the first task is to define which properties are required to make a DSS "weldable", at least under certain conditions. The second task is to identify the more feasible way to empirically verify that such properties are meeting corresponding requirements, and define a methodology supported by standards and practice. Then, the third task is to put everything into practice, demonstrating the weldability of a single DSS by this practical way. Finally, the fourth and last task is generalization, validating proposed methodology by succeeding in applying it for more than a single DSS.

The practical significance of the work carried on in this study is that it was able to close that loop. It determined which properties are required to make a DSS weldable, and at least in equivalent terms the carbon equivalent content method does this. It proposed an alternative holistic methodology to verify such requirements. Finally, it was executed for four different types of welding with four different steels, three DSS and one carbon steel, determining the optimal thermal input and conditions for everyone.

Hence, with the aim of ensuring stainless steel properties, 1.5 mm thickness steel plates will be used for calibration tests to determine the optimum thermal input. These plates are selected as representative of cold-formed corrugated steel to which the standardized range of tests is applicable, including tests on automatic welding and welding beams with no filler metal, considered later on.

The aim here is to minimize the effects of any working variables that do not depend on the material itself avoiding introducing an additional variable relating to material compatibility. Tungsten Inert Gas (TIG) welding was chosen rather than welding, which is also widely used and might be more economical, because TIG welding without filler performs better in terms of corrosion resistance, presenting uniform welding beads and a narrower HAZ [14,15].

In addition to demonstrating the sound weldability of the flat steel plates and sheeting, these calibration tests will serve to verify the competitive properties of the plates when used alongside steel rebars, usually welded together in preassembled meshes to reinforce unique structural components. The flat steel products in the mesh often share the concrete matrix with other carbon steel rebars, placed in peripheral positions and protected only by the corresponding concrete cover. As hybrid specimens, the corrosion resistance tests of these steel products will therefore be representative of their suitability for the structural optimization of mesh reinforcements within the concrete matrices.

Accordingly, for the sake of integrating all the characteristic procedures of industrial welding, the process schedule was as follows:

1. Specimen preparation, border alignment, cleaning, bench placement, etc.
2. Welding of the specimen.
3. Brushing + pickling + passivization.

Hence, the first objective of this research is to define the optimum thermal input of each of the tested duplex stainless steels, i.e., the optimum temperature at the beginning of welding and between passes, which differs a priori for each steel grade.

Thermal input is the most important variable in any definition of properly welded stainless steel, a fact that has been confirmed in multiple studies, including those by Mohammed et al., which concluded that DSS steel 2205 tolerated a higher thermal input than austenitic steels [16], and by Asif et al., which concluded that duplex 2205 stainless steel performed better with a higher thermal input than austenitic steels [17]. Likewise, Tasalloti et al. concluded that lower heat inputs, also for DSS 2205, produced a great disparity in its composition (i.e., Cr, Ni and Mo) [18]. Besides, it is noteworthy that prolonged thermal inputs can improve the performance of welds [19]. Additionally, Asif et al. [17] underlined how lower inputs imply higher fractions of ferrite and severe precipitation of chromium nitrides; this implies a degradation of mechanical properties and corrosion resistance, such as chloride pitting corrosion, typical of marine environments.

Finally, it is worth mentioning the work carried out by Subramanian et al., who carried out an exhaustive analysis of the anode metal to cathode metal ratio and its influence on the degree of galvanic corrosion [20], to be later considered in this study for dissimilar joints. Likewise, the study by Paul et al. should be highlighted, which examined the way excessive polarization can be controlled to avoid pitting and can simultaneously reduce anode consumption [21].

Secondly, after welding with each corresponding optimum input (welding speed, temperature, etc.), the welds were validated by the full range of Non-Destructive Tests (NDT) required for the certification of welding procedures and, likewise, corrosion tests in a salt spray chamber in accordance with EN ISO 9227-NSS [22].

Although studies support the good performance of stainless steel in all types of environments [23], the equilibrium in DSS between ferrite and austenite is necessary for a good performance in marine environments, [24]. Hence, these tests successfully determined which of the DSS welded joints presented the most competitive characteristics for mechanical performance and which of them still behaved well in saline environments.

Additionally, following the same above-mentioned procedures, the feasibility of welding DSS and S275JR, a weldable type of carbon steel, was also analyzed in this research, above all with respect to galvanism. In similar studies, Sternhell et al. [25] showed the anodal role of copper in marine environments and Subramanian et al. analyzed the behavior of zinc with stainless steel in tropical marine environments [20].

Finally, as a last remark, the research value chain presents several stages. In the first stage, the novelty lies in realizing and identifying a problem that need to be solved. Then, the novelty comes when the first solutions to that problem are proposed, and when these solutions are optimized after that. Finally, at the end of the day, the novelty and the research added value still lie in performing it simply and more feasibly in a practical way. Thus, the novelty of this study is presenting an optimized and feasible procedure to determine DSS weldability in practice, alternative to the very simple carbon equivalent method. Furthermore, the novelty also lies in putting it in practice for several DSS, demonstrating simultaneously the weldability of the DSS, the relationship between their optimized thermal inputs, the feasibility of the methodology itself and its generalization for several DSS, effectively closing the loop.

2. Materials and Methods

2.1. Materials

Regarding the used materials, Table 1 shows the results of the DSS chemical composition tests of each steel grade with the aim of assessing the weldability of the different types of DSS and their corrosion resistance in marine environments. Each specimen was formed by two sheets of $180 \times 80 \times 1.5$ mm^3 dimensions, welded together by Tungsten Inert Gas (TIG) welding. Four different specimen types were built up depending on the material of each welded sheet and several samples of each type:

- Pure DSS 1.4482 (2001)
- Pure DSS 1.4362 (2304)
- Pure DSS 1.4462 (2205)
- Hybrid DSS 1.4462 (2205)/carbon steel (S275JR)

Table 1. Chemical composition of duplex stainless steels (%).

Steel	C	Si	Mn	P_{max}	S	Cr	Ni	Mo	N	Cu
2001 LDSS	≤0.03	≤1	4.0–6.0	35	0.03	19.5–21.5	1.5–3.5	0.1–0.6	0.05–0.25	≤1
2304 LDSS	≤0.03	≤1	≤2	35	0.015	22–24	3.5–5.5	0.1–0.6	0.05–0.25	0.15–0.6
2205 DSS	≤0.03	≤1	≤2	35	0.015	21–23	4.5–6.5	2.5–3.5	0.1–0.22	-
S275JR	21	-	1.5	0.035	35	-	0.012	-	-	0.55

2.2. Methods

The research tasks were divided into different stages, as indicated in Table 2. The first step was to determine the optimum thermal input, after this, different specimens were welded and analyzed to determine their welding quality and its behaviour in a marine environment.

Table 2. Research stages.

Stage	Item	Description
S1	Welding	Experimental characterization of the optimum thermal input for each steel grade under TIG welding conditions without filler.
S2	Welding	Performing TIG welds without filler, each material will use its optimal input.
S3	Test	Application of NDT: Visual, penetrating liquids, X-rays
S4	Test	Micrographies, microstructural analysis and ferrite content
S5	Test	Corrosion test in salt spray chamber

The base material for welding the austenitic-ferritic stainless steel was prepared in different dimensions for the post-welding tests.

Figure 1 schematizes weld join design (a) and welding sequence (b) used in each specimen. From a design point of view, a butt weld with full penetration between two 1.5 mm sheets was carried out, without edge preparation and without sheet spacing. Besides, an automatic TIG welding without filler was performed in a single pass from one side and without backing. Accordingly, this minimizes the number of variables of the procedure.

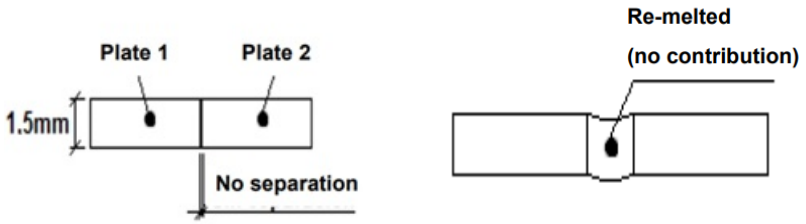

(**a**) (**b**)

Figure 1. Detail of butt weld with full penetration without edge preparation nor sheet spacing: (**a**) cross-section of welded joint design; (**b**) Welding sequences.

Table 3 summarizes the predefined variables used during the welding for the different materials. These variables are identical for the welding of all materials because they are directly associated with the welding process, regardless of the type of material to be welded.

Table 3. Values considered for predefined variables.

Variables	Value
Welding process	T.I.G. (Tungsten Inert Gas. 141)
Mechanization level	Automated
Type of welded joint	Butt weld, Single side, Backless (BW SS NB)
Welding positions	Under hand (PA)
Thickness of base sheet (mm)	1.5 mm
Outside diameter (mm)	N/A
Type of metal filler	No support
Shielding gas	99.9% Argon
Shielding gas flow rate	12 L/min
Shielding Gas Support	99.9% Argon
Support shielding gas flow rate	4 L/min
Type of electricity	Direct Current, Electrode to negative
Minimum preheating temperature	Room temperature (15 °C)
Maximum temperature between passes	N/A
Post-Welding Heat Treatment	N/A
Maximum bead oscillation/width	Straight
Pulsed welding parameters	No
Tungsten electrode, type/diameter	Tungsten + 2% Torio (Red), 2.4 mm
Arc length	3–4 mm
Gun angle	70–80°
Preparation and cleaning method	Initial cleaning: brushing with stainless steel tines Final cleaning: brushing, pickling + passivization
Welding machine	Praxair Triton 2201 AC/DC
Automation equipment	Tractor carriage BUG-O SYSTEMS
Others	Sheet clamping by tools

During stage 2, prior to the welding of the final coupons, a series of welding tests were performed to check the behavior of each base material. The purpose of these tests was to weld the coupons of each base material with different thermal inputs and to assess their specific inputs, thereby obtaining

metallic welding continuity and adequate penetration through the root zone. This input should result in welds without plate perforation due to excessive input, while also avoiding the lack of fusion because of insufficient input.

Variables defined in Table 3 were the same for each specimen; however, thermal input depends on the material of specimens, so specific thermal input was defined for each specimen. Besides, it depends on current intensity, voltage, and welding speed. Thus, the following Equation (1) was used for the calculation of the thermal input, where Q is the derived thermal input in J/mm, I is the current intensity in Amperes, V is the voltage in Volts, and S_w is the welding speed in mm/s. For this study 100 A current density was defined; arc length defines voltages, considering an arc length of 3–4 mm (as Table 3 summarizes) means a voltage of 11–11.5 V.

$$Q = \frac{I \cdot V}{S_W} \tag{1}$$

The coupons were welded at different speeds, using the option provided by the equipment to regulate the speed, see Figure 2. In this way, the welding was performed with different thermal inputs and the corresponding results were compared and analyzed to define the optimum one. Initial tests showed that 2001 LDSS resists lower thermal input before drilling than 2304 LDSS and 2205 LDSS while 2304 LDSS resist a little bit more thermal input than 2001 LDSS and 2205 DSS a little bit more than 2304 LDSS. Thus, 11 tests were carried out only to optimize the thermal input of 2001 LDSS and, taking this as a reference, the thermal input was slightly increased step by step for 2304 LDSS and 2205 LDSS thereafter, until reaching their own optimum input.

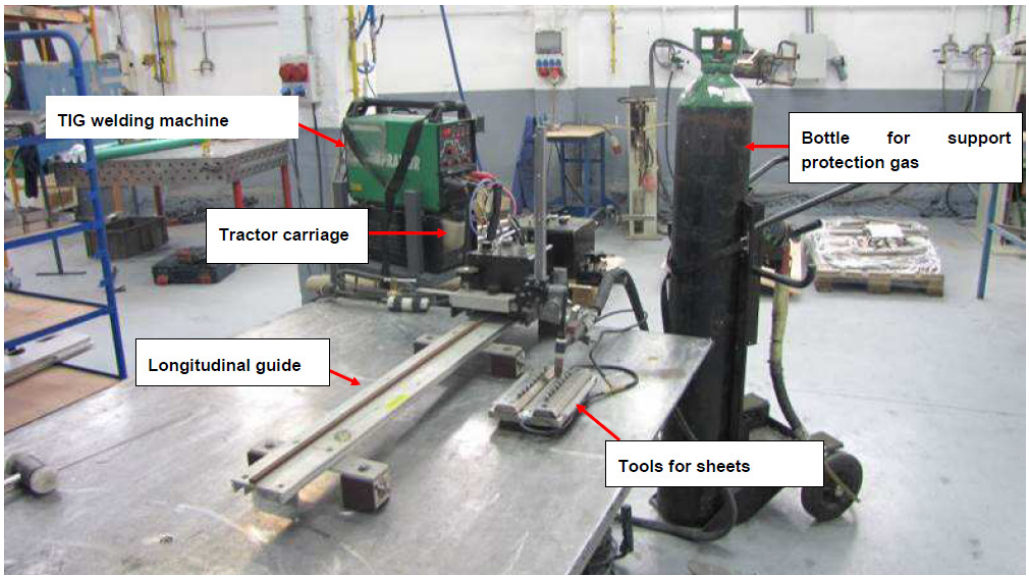

Figure 2. Automatic welding equipment: including sheet tooling, traction carriage on longitudinal guide rail to automatically control welding speed, Tungsten Inert Gas (TIG) welding machine to apply constant thermal input parameters, and shielding gas connection to perform welding under inert gas.

Thermal input also can be defined from nickel equivalent and chromium equivalent numbers. For instance, using the Schaeffler equation [26], a direct relationship can be derived between the summation of equivalent nickel and equivalent chromium of each DSS steel grade and the corresponding optimal thermal input of its welding seams. See Equation (2).

Then, once each coupon was welded at different welding speeds, the weld seam and adjacent area was pickled and passivated, to restore the corrosion resistance properties of the steel after welding and grinding. A pickling and passivation paste was used for this purpose. Figure 3 shows the coupons

following this treatment process. Finally, following the application of these restorative treatments, the saline spray tests were performed to ensure post-welding corrosion resistance.

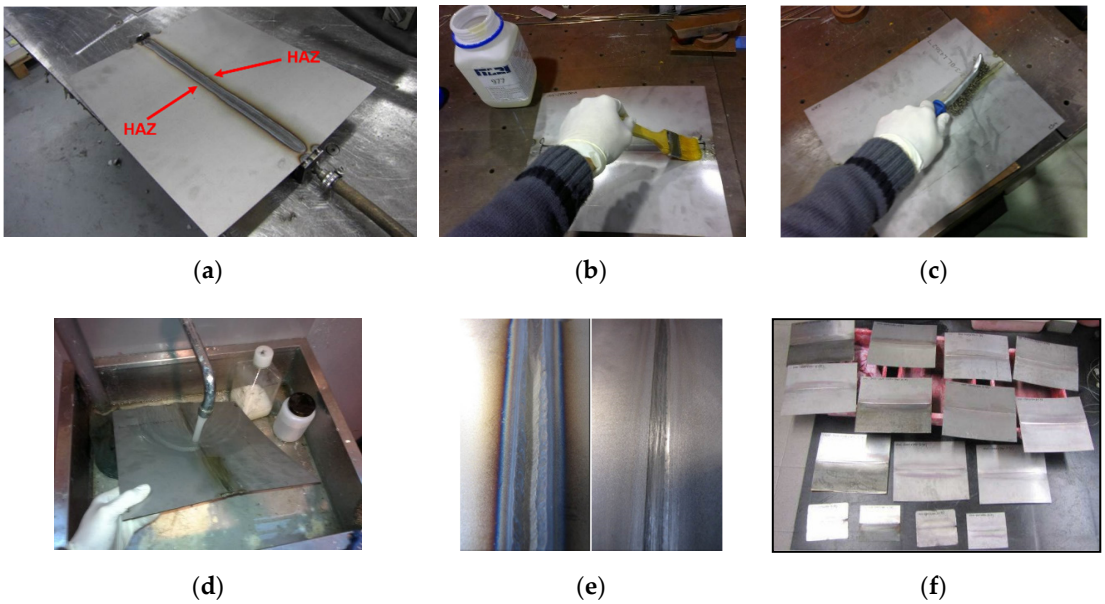

Figure 3. Welded coupons for testing, already prepared after pickling and passivation: (**a**) Detail of the HAZ appearing after welding; (**b**) Application of pickling and passivation product; (**c**) Removing the pickling and passivation product; (**d**) Sample and weld seam cleaning; (**e**) Comparison of the welded seam before and after pickling and passivation; (**f**) Welded coupons prepared for testing.

Every coupon was then analyzed by non-destructive tests (NDT) to determine the optimal thermal input for each steel as the minimum thermal input required for welding without any fault, according to the following standards.

- Visual test: as per standard ISO-17637:2011 [27], in replacement of standard EN-970:1997 [28].
- Test for the detection of surface cracks by penetrating liquids: as per standard EN-571-1:1997 [29].
- Radiographic test: as per standard EN-1435:1998 [30].

Besides, standard EN 5817 [31] was used for the result assessment; the standard defines three different quality level (D,C,B) on the basis of type, size and amount of selected imperfection. B means the highest quality and D the lowest. Accordingly, only B level was accepted in this study

The tests to derive ferrite content is based on ASTM E562 standard [32]. In order to evaluate the welded joints, the following specimen preparation and test application tasks are applied:

1. Saw cutting, in a mechanical workshop, of welding section.
2. Specific preparation of specimens, at the laboratory level, by embossing the samples in resin and mirror polishing.
3. Electrolytic attack of samples using 40% NaOH soda, to calculate the ferrite content on micrographies,
4. Electrolytic attack of samples by 10% oxalic acid, for microstructural observation in light microscope.

These tests are followed by destructive neutral salt spray (NSS) according to ISO 9227 [22]. Therefore, the samples were sprayed in a 5% sodium chloride solution within the pH range of 6.5 to 7.2 in a controlled environment, with an exposure duration up to 216 h. Figure 4 shows the coupons placed inside test chamber

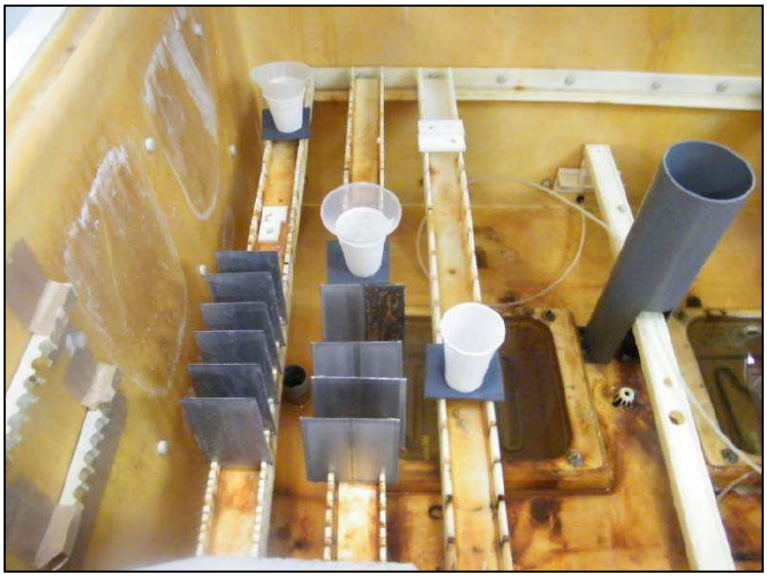

Figure 4. Samples of Tungsten Inert Gas (TIG) welded stainless-steel sheets (2001, 2304, 2205 and S275-2205) during the application of the marine corrosion test in a salt spray chamber.

3. Results

This section discloses the results of the NDT for determination of optimized thermal input of each steel joint type, the results regarding the ferrite content by means of micrographies and microstructural analysis and the results of the salt spray chamber destructive tests.

3.1. Optimized Thermal Input

The process for the determination of thermal input of DSS 2001 is analyzed below. The process followed for the other materials was the same.

As mentioned before, the voltage derived from the applied arc height ranged from 11–11.5 V. A mean voltage of 11.25 V was taken into account for the calculation of the thermal input by Equation (1). A total of 11 DSS coupons were welded. Table 4 summarizes the thermal input value used for each specimen relating to 1.4482 (2001) DSS coupons.

Table 4. Therma input used for each coupon of 1.4482 (2001).

Ref. Coupon	Q (kJ/mm)
2001 × 180-A	0.256
2001 × 180-B	0.188
2001 × 180-C	0.150
2001 × 180-D	0.138
2001 × 180-E	0.321
2001 × 180-F	0.275
2001 × 180-G	0.307
2001 × 180-H	0.181
2001 × 180-I	0.231
2001 × 180-J	0.245
2001 × 180-K	0.281

For 2001 × 180-D and 2001 × 180-E coupons, the penetrating liquid and radiography tests were not applied, since they presented lack of root penetration and perforation, respectively, during visual examination. A and G coupons failed to pass the evaluation of the radiographic test, due to detected internal fusion faults. The remaining coupons met the requirements of the radiographic test. However,

visual observation of the weld-seam surface should also be considered. See Figure 5 showing X-ray and penetrating liquids NDT procedure for some samples.

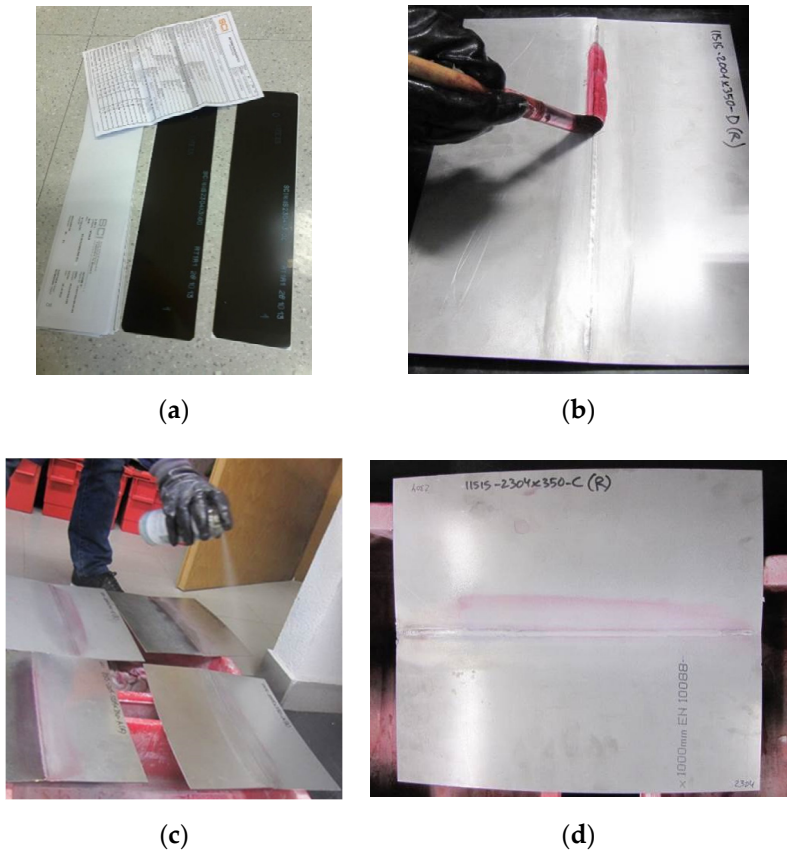

Figure 5. X-ray and penetrating liquids non-destructive testing performed on samples: (**a**) X-ray plates and test certificates of samples; (**b**) Application of penetrating liquids in red; (**c**) Application of revealing product after cleaning; (**d**) 2304 Duplex Stainless Steel (DSS) sample showing a good result with no penetration.

Following the completion of the radiographic test, a visual examination of the coupon welding surfaces was completed (Figure 6 shows the status of some welded specimens). The weld seam surface of coupon "2001 × 180-K" was unstable and irregular, with a sinusoidal weld along the entire joint. 2001 × 180-F coupon ref. showed a longitudinal contraction towards the inside of the seam on the welding side; this contraction appeared to be a kind of root concavity defect. Coupon "2001 × 180-J" was welded with a slightly lower thermal input than the coupon "2001 × 180-A". The surface showed an irregular and sinusoidal weld. It was therefore discarded as a non-optimal weld. The seam on coupon ref. "2001 × 180-B" showed an irregularly shaped bead at the welding face side, so the solidification of the seam is not optimal and could be improved. On the other hand, coupons with ref. "2001 × 180-H" and "2001 × 180-C" showed an excessively narrow weld seam width in the root area. This effect is attributed to the application of an excessively high welding speed on both coupons, and therefore, an excessively low thermal input. Table 5 summarizes radiographic results.

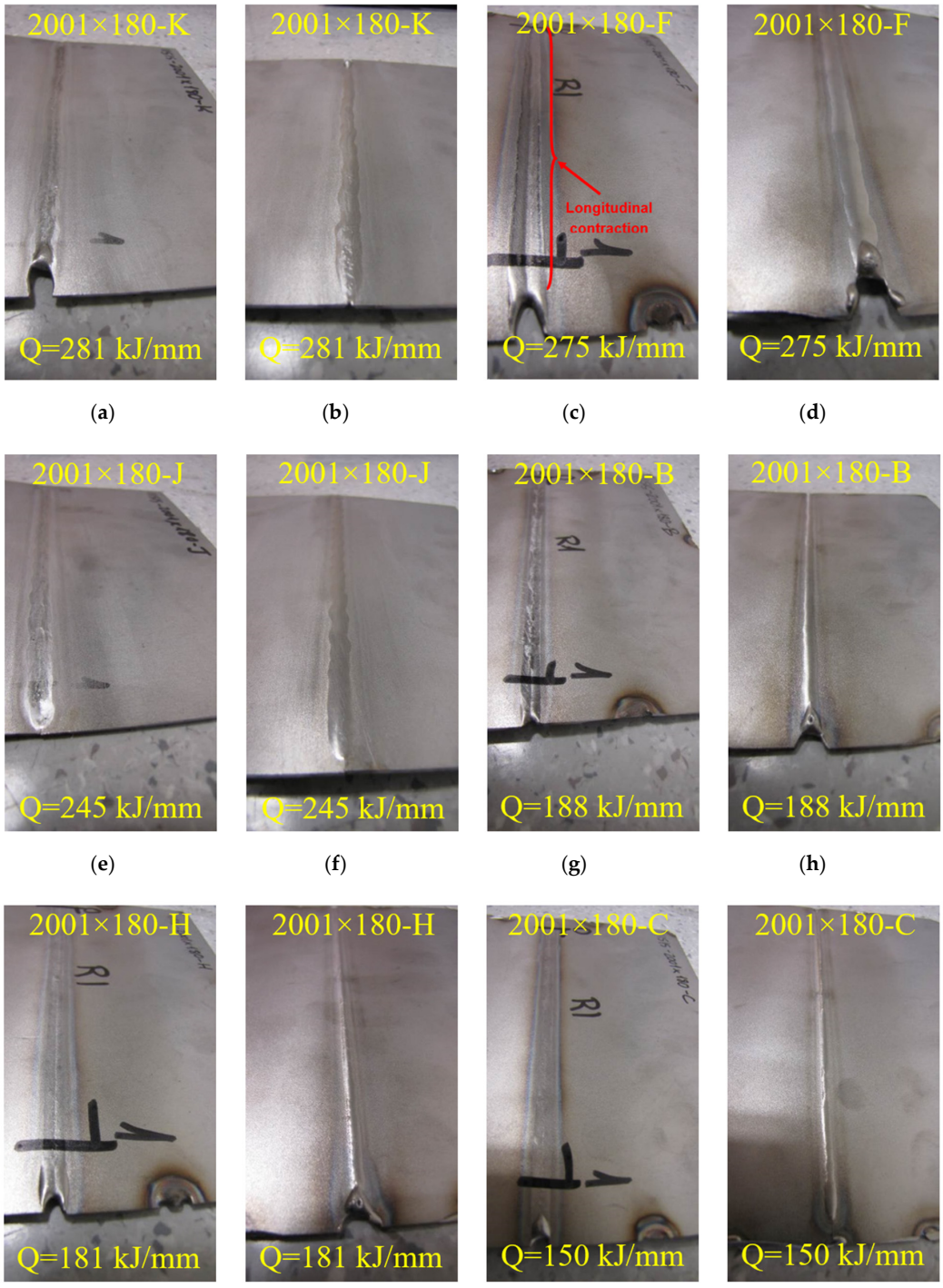

Figure 6. Welded coupons of 2001 steel from welding face and root sides: (**a**) 2001 × 180-K from the welding face side (Q = 281 kJ/mm); (**b**) 2001 × 180-K from the welding face side (Q = 281 kJ/mm); (**c**) 2001 × 180-F from the welding face side (Q = 275 kJ/mm); (**d**) 2001 × 180-F from the welding face side (Q = 275 kJ/mm); (**e**) 2001 × 180-J from the welding face side (Q = 245 kJ/mm); (**f**) 2001 × 180-J from the welding face side (Q = 245 kJ/mm); (**g**) 2001 × 180-B from the welding face side (Q = 188 kJ/mm); (**h**) 2001 × 180-B from the welding face side (Q = 188 kJ/mm); (**i**) 2001 × 180-H from the welding face side (Q = 181 kJ/mm); (**j**) 2001 × 180-H from the welding face side (Q = 181 kJ/mm); (**k**) 2001 × 180-C from the welding face side (Q = 150 kJ/mm); (**l**) 2001 × 180-C from the welding face side (Q = 150 kJ/mm).

Table 5. Radiographic results and observations depending on the thermal input.

Ref. Coupon	Q [kJ/mm]	Radiography Test	Remarks
2001 × 180-E	321	Not applicable	Drilling
2001 × 180-G	307	Not acceptable	X-ray: Lack of internal fusion
2001 × 180-K	281	OK	Irregular weld seam
2001 × 180-F	275	OK	Longitudinal contraction per side
2001 × 180-A	256	Not acceptable	X-ray: Lack of internal fusion
2001 × 180-J	245	OK	Irregular weld seam
2001 × 180-I	231	OK	Weld seam without relevant indications
2001 × 180-B	188	OK	Weld bead that can be improved per face area
2001 × 180-H	181	OK	Excessively narrow weld bead per root
2001 × 180-C	150	OK	Excessively narrow weld bead per root
2001 × 180-D	138	Not applicable	Lack of root penetration

According to the results from the visual inspection, liquid penetration test and radiographic test, I coupon was defined as the optimum weld with a thermal input of 0.231 kJ/mm. Table 6 summarizes the optimal thermal input obtained by the same procedure for different materials and parameters used in weld process.

Table 6. Summary of welding parameters and corresponding optimized thermal input.

MATERIAL	I (A)	V_{mean} (V)	Forward Speed (mm/s)	Q (kJ/mm)
2001	100	11.5	4.86	0.231
2304	100	11	3.76	0.293
2205	100	11.75	3.67	0.320
2205-S275	100	12	3.61	0.332

3.2. Ferrite Content

Prior to the microstructural analysis, a macrograph of each type of material is taken, in which base materials are observed, with corresponding heat affected zones (HAZ) and the weld.

Subsequently, a microstructural analysis is carried out including images of the cord, the HAZ and the base material. At least six micrographs are obtained for each type of material at ×400 magnification. The ferrite content and the possible presence of intergranular precipitates are analyzed. Thus, two types of micrographs are obtained:

- Micrographs of samples electrolytically etched with 40% NaOH soda: for the calculation of the ferrite content. These micrographs are displayed in color. Austenite is visualized in white, and ferrite in color.
- Micrographs of samples electrolytically attacked with 10% oxalic acid: for microstructural observation in an optical microscope (possible precipitates, intermetallic phases, etc.). These micrographs are displayed in black and white.

3.2.1. Macrographies

Figure 7 discloses the macrographies of the cross section corresponding to the four steel joint types belonging to 2001, 2304, 2205 and 275-2205 base materials. Each shows a correct welding zone with minimum drop to the root and clearly showing different aspects for the welding, base material and HAZ transition zones that indicate the presence of different phases and material inclusions. Therefore, since the welding can act as a thermal treatment evaporating the protective elements of the stainless steels disclosed at Table 1 and changing its microstructure, a micrography and microstructural analysis is required to ensure the welding process is not depriving the corrosion resistance of such materials to marine environments full of chlorides.

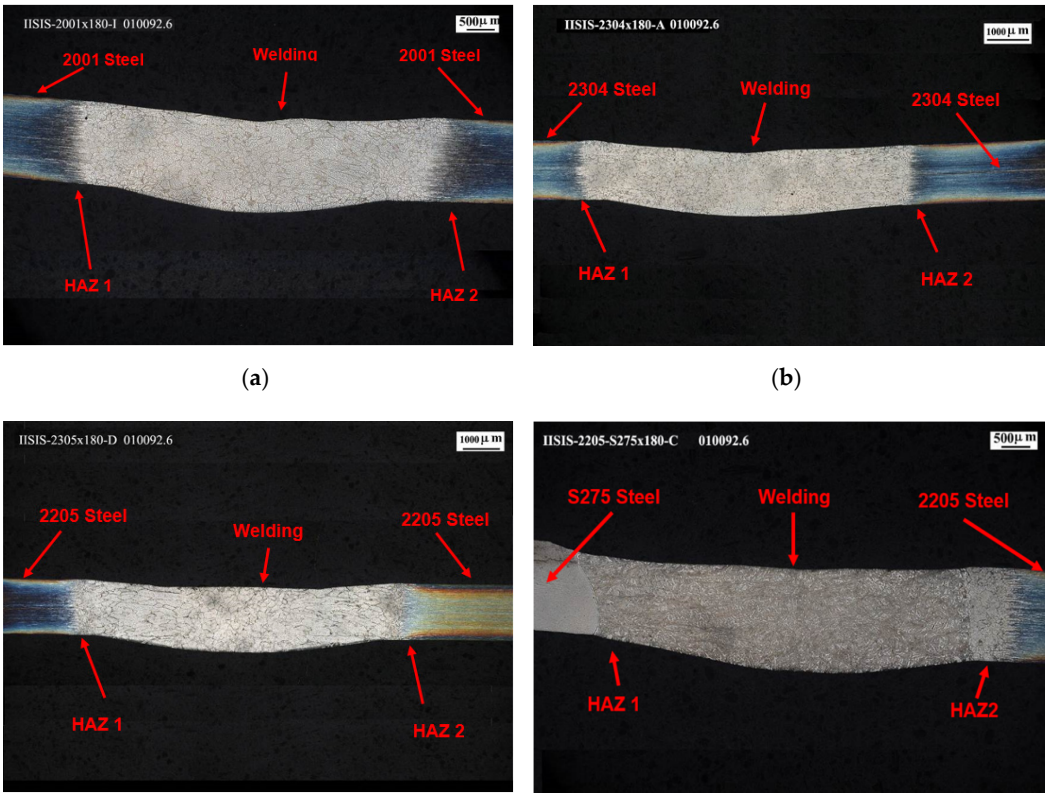

Figure 7. Cross-Section welded joint macrographies: (**a**) 2001-2001 steel joint with ×12 Magnification; (**b**) 2304-2304 steel joint with ×9 Magnification; (**c**) 2205-2205 steel joint with ×8 Magnification; (**d**) 275-2205 steel joint with ×9 magnification.

3.2.2. Micrographies

As already mentioned, the micrographies have been performed on previously etched samples with 40% NaOH soda. These micrographs are displayed in color, with austenite shown in white, and ferrite is colored. Accordingly, Table 7 summarizes the ferrite content obtained for each welded coupon after applying the test, depending on the zone.

Table 7. Ferrite content of each optimized coupon (%).

Reference	Base Steel	HAZ	Welding
2001 × 180-I	53.0	68.4	73.5
2304 × 180-A	55.6	71.6	82.4
2205 × 180-D	59.8	74	86.3
2205-S275 × 180-C	60.2	72.5	47.5

Besides, Figures 8–11 show the micrographies with ×400 magnification of the four steel joint types considered in this study. As general remarks for all cases, ferrite and austenite bands can be seen in the base material, and are elongated in the direction of the sheet hot-rolling. In welding zones, an increase in the percentage of ferrite is appreciated when compared to the base material, and it can be observed the presence of acicular austenite too. The same is applicable for the HAZ, in which the grains present a greater orientation to the hot rolling direction at the area closest to the base material (left).

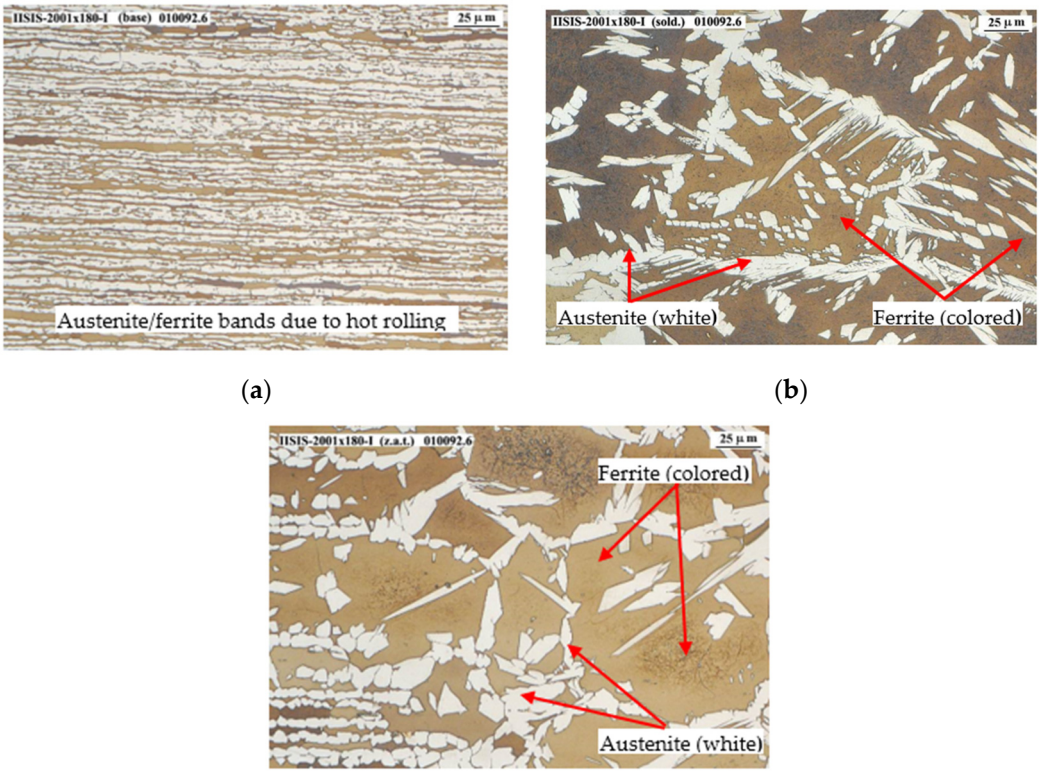

Figure 8. 2001-2001 steel joint micrographies: (**a**) Base 2001 steel with ×400 magnification; (**b**) Welding zone with ×400 Magnification; (**c**) 2205 HAZ zone with ×400 magnification.

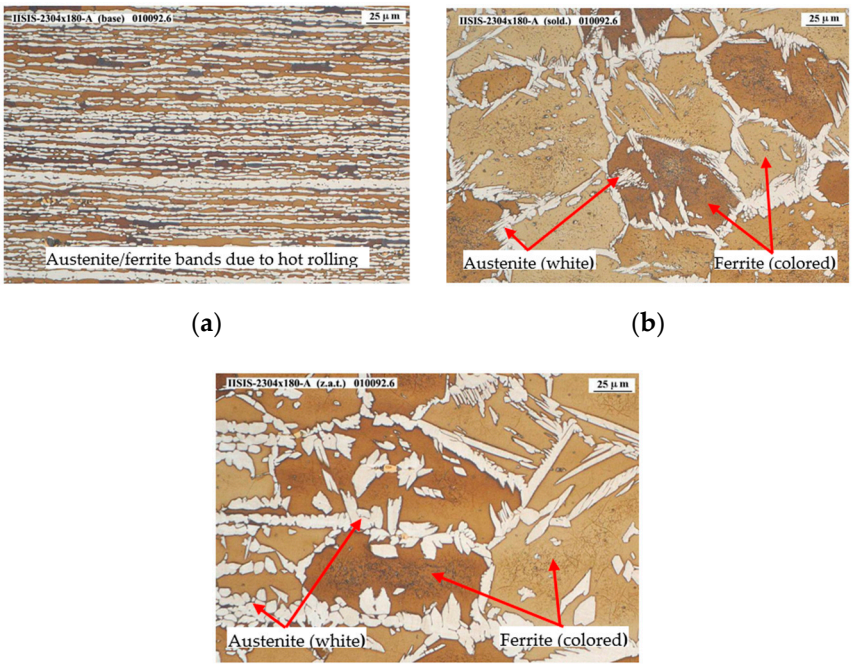

Figure 9. 2304-2304 steel joint micrographies: (**a**) Base 2304 steel with ×400 magnification; (**b**) Welding zone with ×400 Magnification; (**c**) HAZ zone with ×400 magnification.

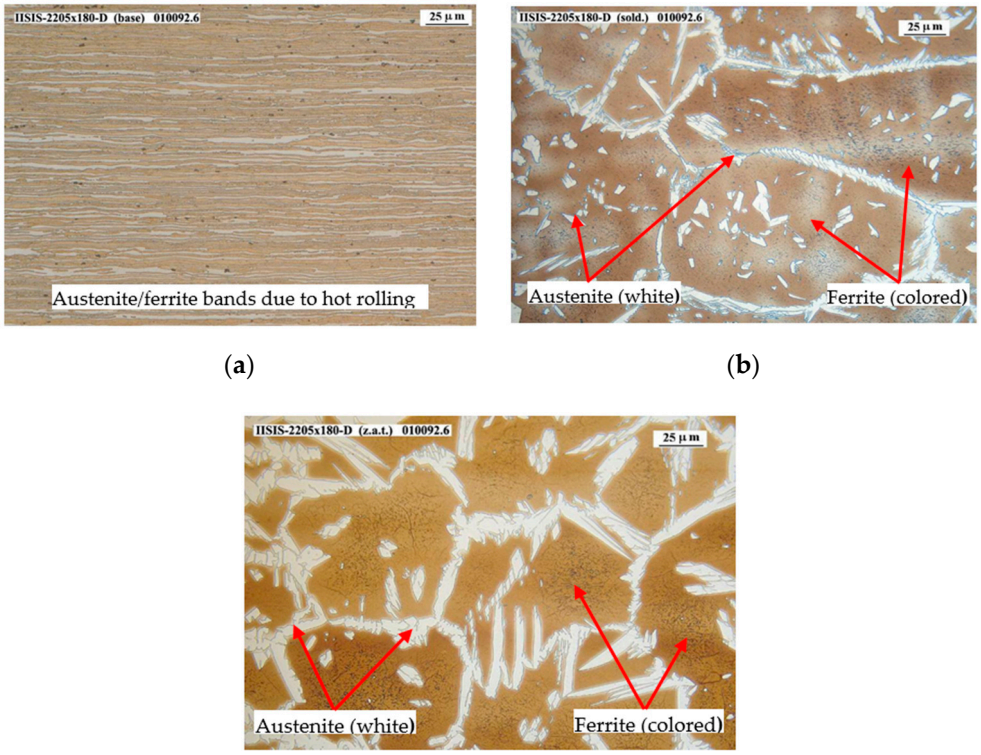

(**a**) (**b**)

(**c**)

Figure 10. 2205-2205 steel joint micrographies: (**a**) Base 2205 steel with ×400 magnification; (**b**) Welding zone with ×400 Magnification; (**c**) HAZ zone with ×400 magnification.

Additionally, for the hybrid 275-2205 steel joint, see Figure 11, the ferrite appears in orange in the area of 2205 base material and corresponding HAZ. Nevertheless, the ferrite appears bluish in welding area. This difference in color is due to the fact that in the welding area, as no filler material has been used, there has been a dilution between the austeno-ferritic material 2205 and the carbon steel S275, and when this area is attacked with soda, the ferrite has reacted turning blue.

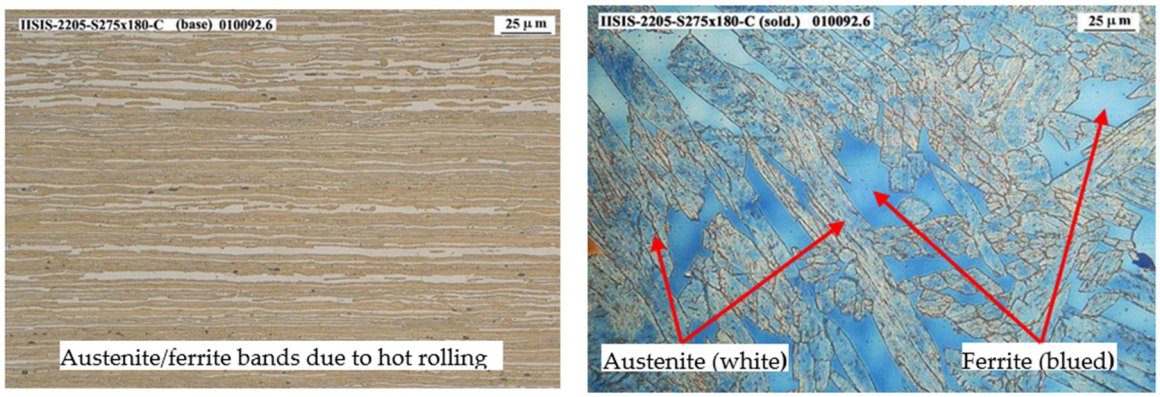

(**a**) (**b**)

Figure 11. *Cont.*

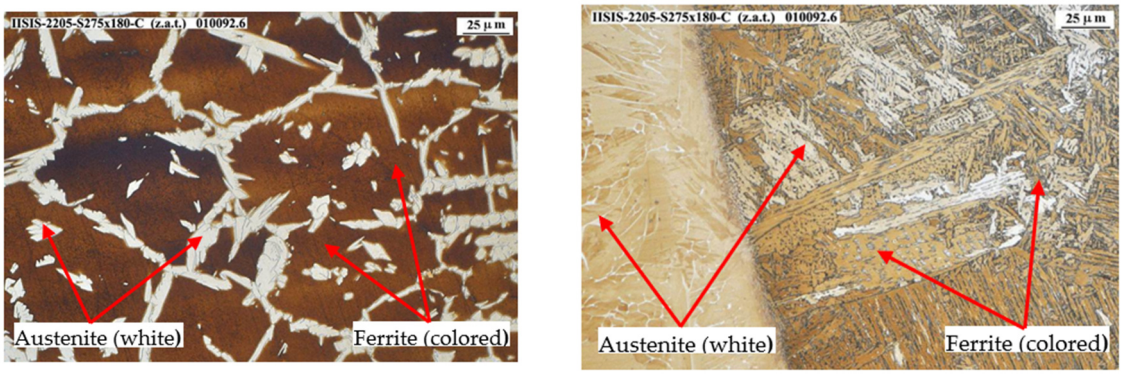

(**c**) (**d**)

Figure 11. 275-2205 steel joint micrographies: (**a**) Base 2205 steel with ×400 magnification; (**b**) Welding zone with ×400 Magnification; (**c**) 2205 HAZ zone with ×400 magnification; (**d**) S275 HAZ zone with ×400 magnification.

3.2.3. Microstructural Analysis

The next micrographs have been performed on samples electrolytically attacked with 10% oxalic acid to enable the microstructural observation in an optical microscope (possible precipitates, intermetallic phases, etc.). Accordingly, these micrographs are displayed in black and white, see Figures 12–15, where ferrite shows a dark color and austenite a lighter one.

As an additional clarification, this kind of micrograph is used to look for possible indications of the presence of precipitates, intermetallic phases, sigma or chi phases and the like. These indications take the form of discontinuities with surrounding metallic structures. Nevertheless, despite it being a good way to see if a certain sample shows enough of such indications, it is not suitable to determine the nature of the discontinuity itself. For that purpose, the scanning electron microscope (SEM) is used as a complementary tool to complete the analysis instead. Thus, typically the more cost-effective strategy is to first analyze the samples already attacked with 10% oxalic acid in search of indications to determine the usefulness of a further SEM analysis or lack thereof, discarding it or not accordingly.

However, the micrographs of this study have shown a rather low and scarce amount of such indications, meaning almost no presence of possible precipitates or intermetallic phases. The red circles in some of the next figures just show places of special interest because of the possible presence of such indications. Nevertheless, after a further study of such places, it was considered that micrographs were not presenting enough evidence to make a SEM study advisable, discarding it accordingly.

Figure 12a–c shows the micrographies corresponding to 2001 base material, welding and HAZ zones, respectively. In these last two zones, precipitates or intermetallic phases are appreciated in some areas of the grain edges, in small quantities, such as the sigma phase or the chi phase. It should be mentioned that the appearance of the sigma phase cannot be confirmed by optical microscope means only, but rather a SEM would have to be used. However, the number of indications detected is considered low, so that even with SEM electron microscope analysis it would be difficult to define the nature of these indications.

For 2304 steel, a slightly higher quantity of this type of indications can be seen than in the 2001 material, but is equally scarce, so that even with the analysis by SEM electron microscope it would be difficult to analyze the nature of said indications. See Figure 13.

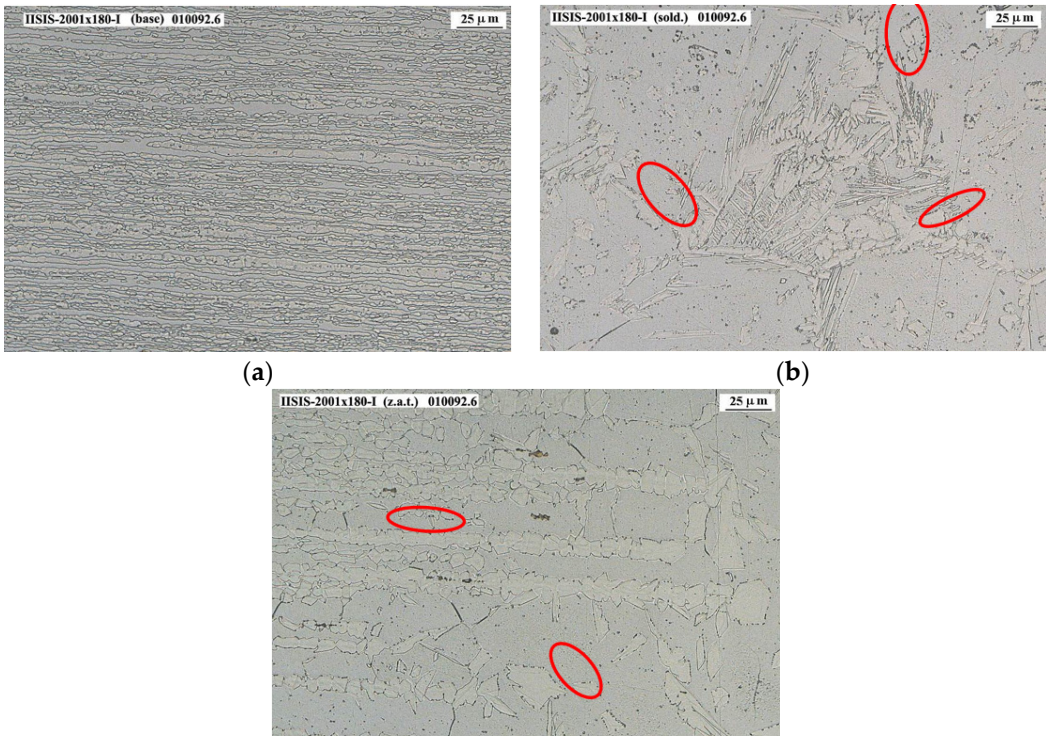

Figure 12. 2001-2001 steel joint micrographies: (**a**) Base 2001 steel with ×400 magnification; (**b**) Welding zone with ×400 Magnification; (**c**) HAZ zone with ×400 magnification.

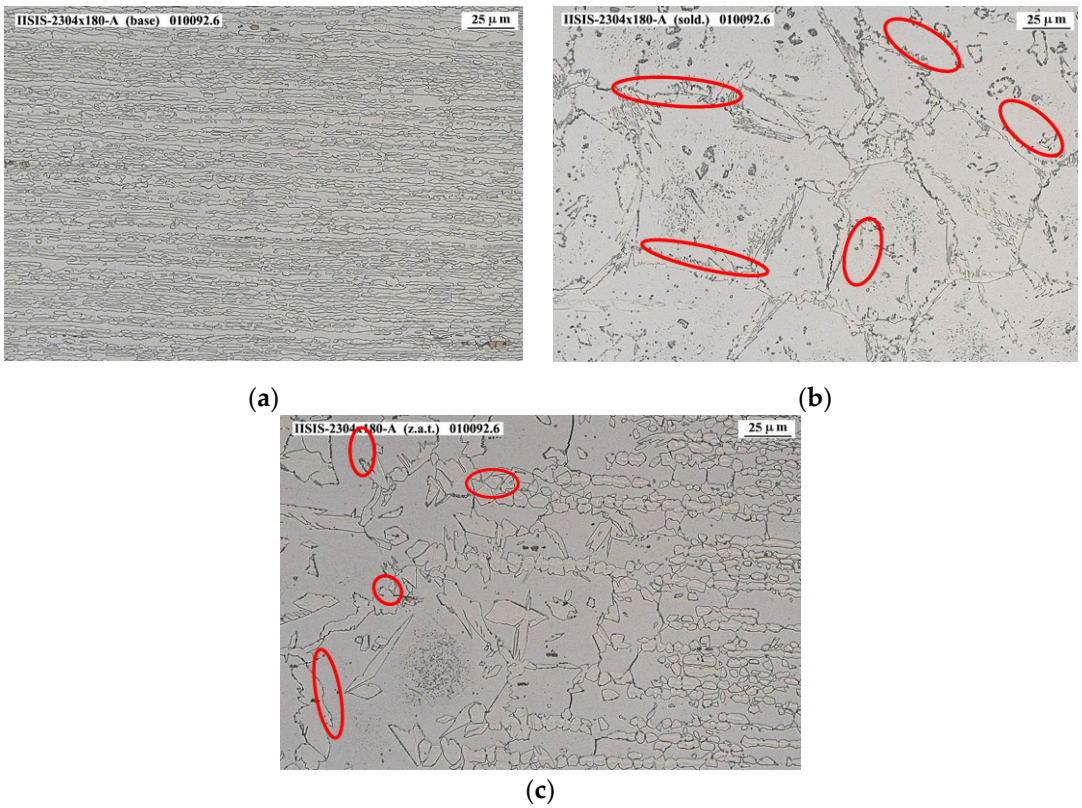

Figure 13. 2304-2304 steel joint micrographies: (**a**) Base 2304 steel with ×400 magnification; (**b**) Welding zone with ×400 Magnification; (**c**) HAZ zone with ×400 magnification.

For 2205 steel, a lower amount of this type of indications is seen than in materials 2001 and 2304, see Figure 14.

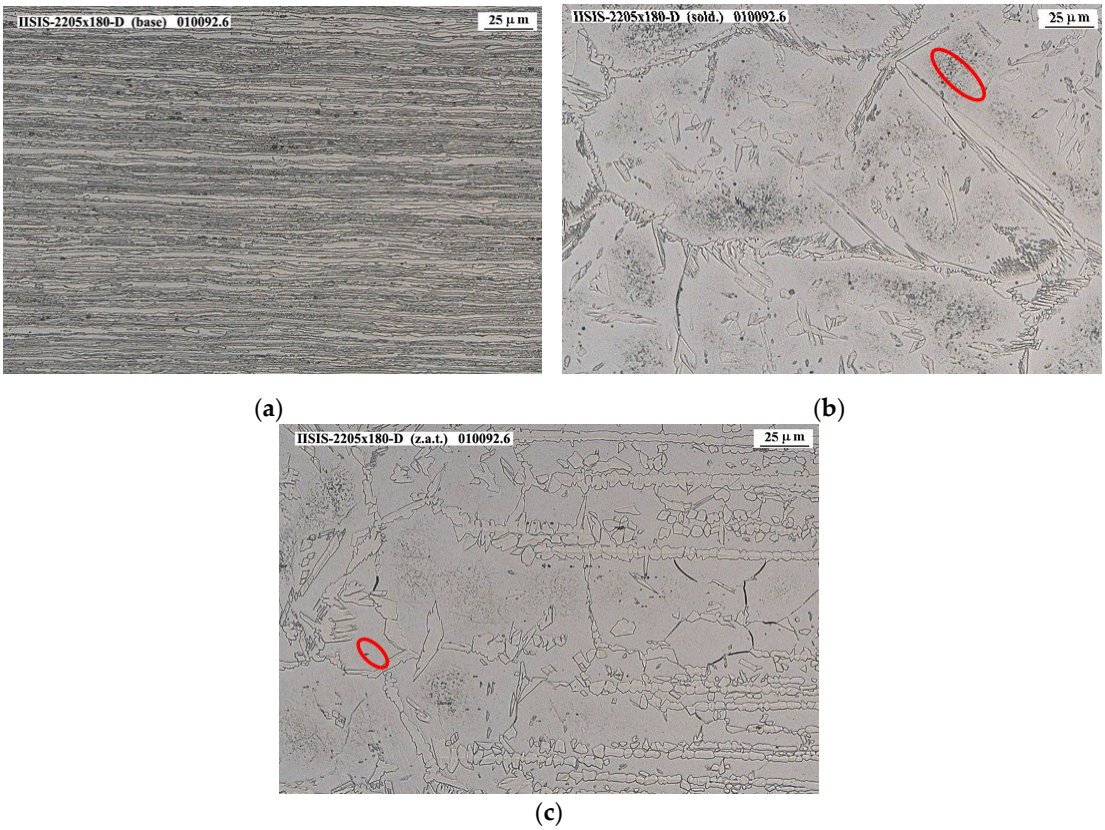

Figure 14. 2205-2205 steel joint micrographies: (**a**) Base 2205 steel with ×400 magnification; (**b**) Welding zone with ×400 Magnification; (**c**) HAZ zone with ×400 magnification.

Finally, a lower amount of this type of indications is appreciated in S275-2205 joint than in the materials 2001 and 2304 and a similar amount to that appreciated in the coupon of material 2205. See Figure 15.

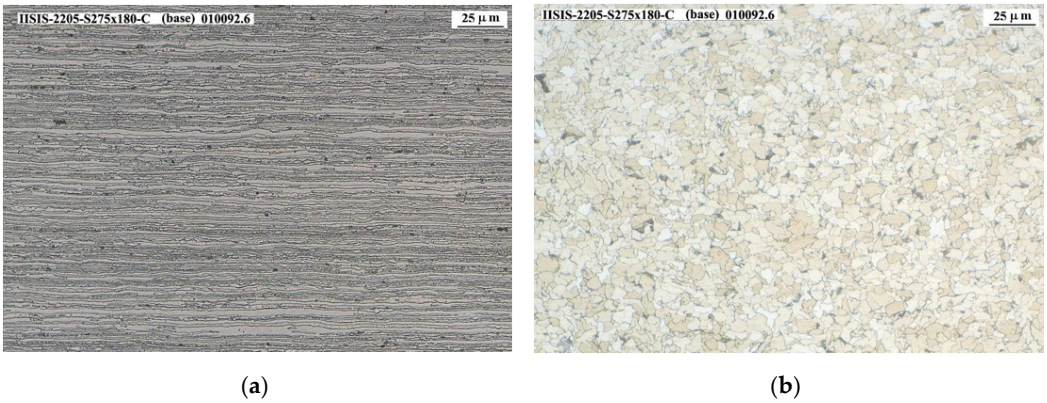

Figure 15. *Cont.*

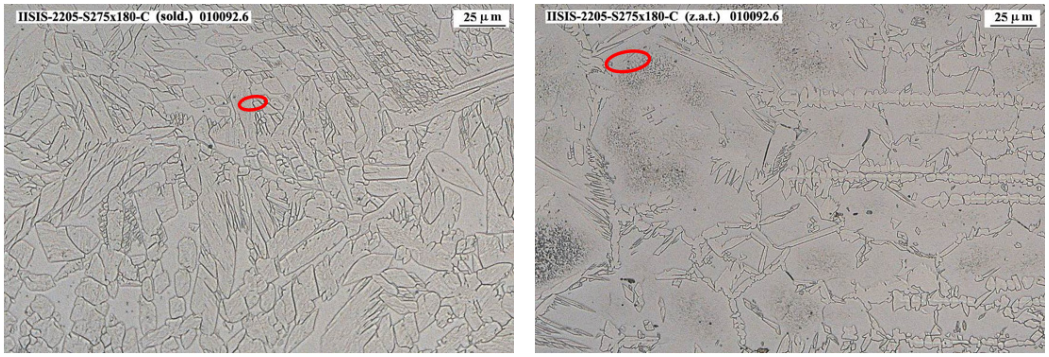

(**c**) (**d**)

Figure 15. 275-2205 steel joint micrographies: (**a**) Base 2205 steel with ×400 magnification; (**a**) Base 275 steel with ×400 magnification; (**c**) Welding zone with ×400 Magnification; (**d**) HAZ zone with ×400 magnification.

3.3. Salt Spray Chamber Test

During this test, the samples were exposed to a harsh environment in a climatic chamber. Thus, after 216 h of exposure to an environment with 5% sodium chloride at a pH ranging from 6.5 to 7.2, it was observed that the welded samples of DSS materials under refs. '2304 × 180-A', '2205 × 180-D' and '2001 × 180-I' remained in perfect state, unaffected by corrosion. See Figure 16.

Conversely, the sample weld between DSS 2205 and the carbon steel, S275, under ref. '2205-S275 × 180-C' showed a continuous progression of red chloride corrosion in the S275 carbon steel area. See Figure 17. According to salt-spray chamber standardized testing procedure, the corrosion stages need to be checked after 24, 48, 168 and 216 h, and the results can be summarized in next steps:

- 24 h: Red corrosion on the right side of the weld. Additionally, a red corrosion spot on the left surface.
- 48 h: No significant variations, progression of red corrosion front to the left surface.
- 168 h: No significant variations, progression of red corrosion front to the left surface continues growing.
- 216 h: Spalling and mass loss due to progression of red corrosion.

Therefore, according to the results, the welding of DSS appears suitable for structural elements placed under marine environments when such welding is done with the proper thermal input. However, the welding of such DSS with carbon steel is not advisable, as it turns the carbon steel into a sacrificial anode. In view of such a result, those steels can be considered as weldable DSS steels, even though they surpass the equivalent carbon maximum content defined in current standards.

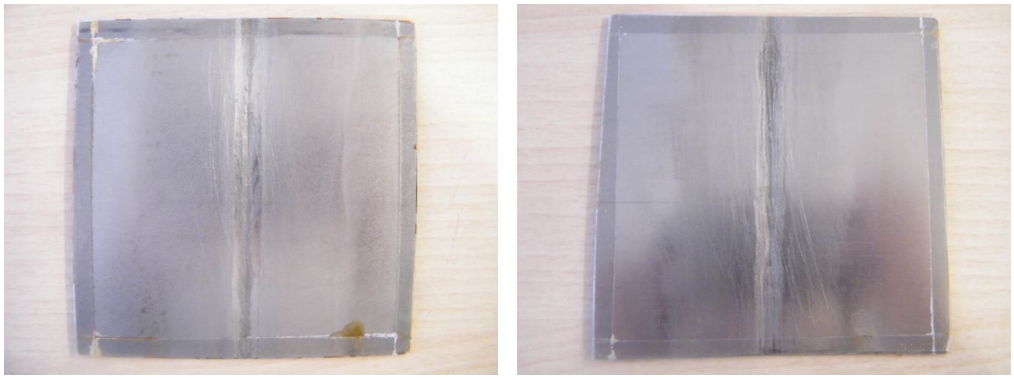

(**a**) (**b**)

Figure 16. *Cont.*

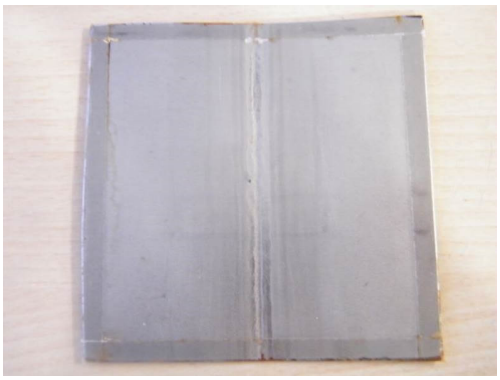

(**c**)

Figure 16. DSS welded samples under simulated marine environment in salt-spray chamber test after 216 h of exposition: (**a**) 2304 DSS showing no significative variations; (**b**) 2205 DSS showing no significative variations; (**c**) 2001 DSS showing no significative variations.

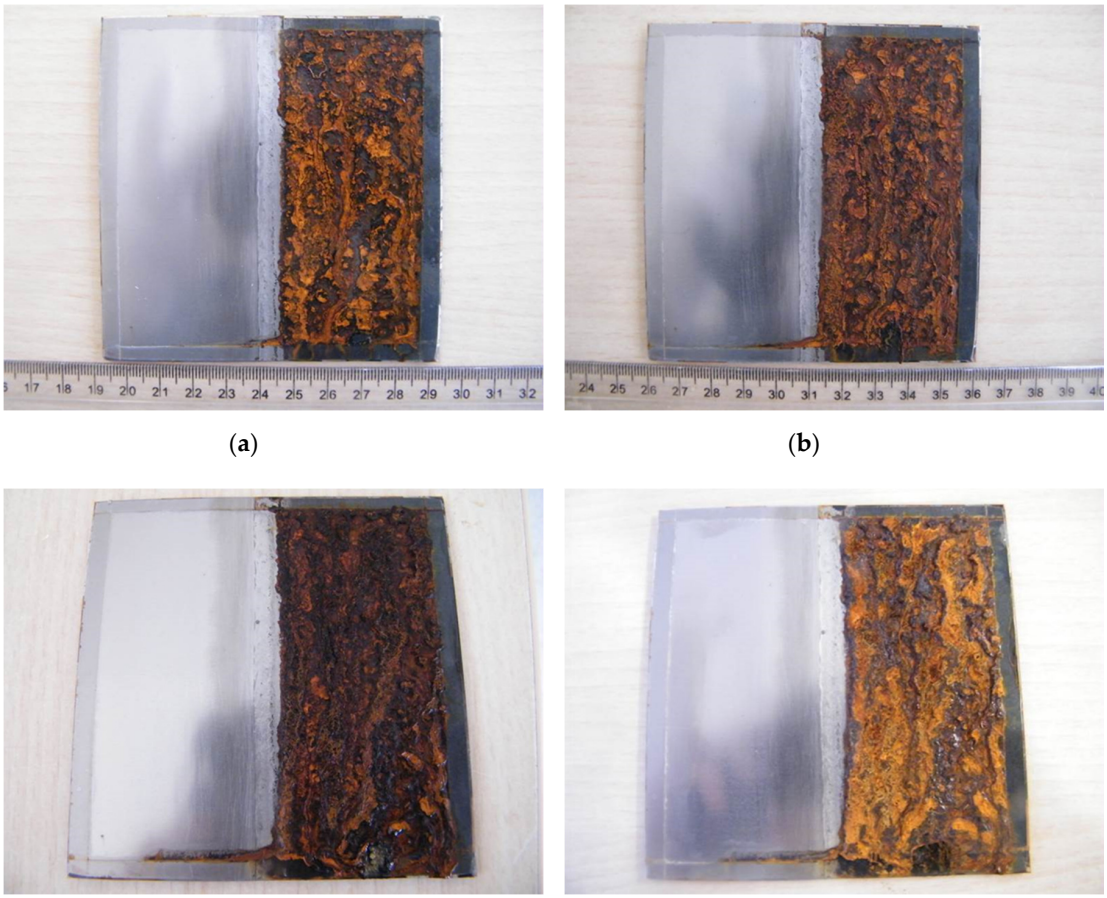

(**a**) (**b**)

(**c**) (**d**)

Figure 17. Hybrid 2205-S275 welded sample under simulated marine environment in salt-spray chamber test: (**a**) After 24 h of exposition showing corrosion at S275 carbon steel; (**b**) After 48 h of exposition showing corrosion progression; (**c**) After 168 h of exposition; (**d**) After 216 h of exposition showing corrosion at S275 carbon steel with aggravated mass loss and small progression towards 2205 steel.

4. Discussion

First, in view of the results disclosed in previous section, every steel joint type was able to be executed at a certain optimized thermal input that was found during the tests. This optimized thermal input is the minimum input required to ensure a suitable and faultless welding seam according to NDT (visual examination, penetrating liquids and radiographic means). Nevertheless, in case of DSS needing to resist chloride corrosion when exposed to a marine environment, there is a risk that such welding processes could cause a protective element loss and ferrite formation weakening the welding and heat affected zones. The higher the thermal input, the higher the risk, so a minimum thermal input while still enough to ensure correct welding is a key founding, but it also requires additional verification of the ferrite formation and remaining corrosion resistance after welding.

Hence, macrographies and micrographies for microstructural analysis have been performed and the results show clearly separated zones corresponding to base metal, HAZ and welding zone, see Figure 7. Ferrite content in base steel was found to be around 53–60%, with 68–72% at HAZ and 73–86% at welding zone. However, an unexpected decrease in the percentage of ferrite is observed in the welding zone of S275-2205 hybrid steel joint in comparison with the austenitic-ferritic base material 2205, up to 47.5%, due to the dilution between both base materials because of the welding without filler, that turned that micrograph to blue instead, see Figure 11b.

Nevertheless, despite the unavoidable rise in ferrite percentage caused by the welding process, although mitigated by optimized thermal input, every DSS still counts on the protective elements in their chemical composition, see Table 1, that protect it from corrosion. Thus, the true performance of each weld needs to be tested in corrosion scenario to see how well each welded joint behaves to corrosion. Accordingly, salt-spray chamber tests have been performed on each steel joint, finding that every steel joint conserve their corrosion resistance with the only exception of the hybrid steel joint S275-2205. In the case of this last joint, the early corrosion attack at the S275 steel half up to the welding seam showed a possible sacrificial anode behavior and the key aspect of the remaining protective elements of DSS after welding, since despite the much lower ferrite content, it showed accelerated corrosion.

Second, adapting the Schaeffler formula [26] with the data gathered in Table 8, obtained directly from DSS chemical composition already disclosed in Table 1, shows a well fitted relationship between the summation of equivalent nickel Ni_{eq} and equivalent chromium Cr_{eq} of each DSS steel grade with the corresponding optimal thermal input of its welding seams. It shows a good correlation under the initial boundary conditions, i.e., butt welding of two narrow 1.5 mm thick steel sheets with full penetration and neither spacing nor edge preparation. Thus, Figure 18 shows the linear regression performed to derive the terms of Equation (2).

Following this procedure, the optimal thermal input Q in KJ/mm of any DSS can therefore be derived from Equation (2), simply by introducing the summation of equivalent Chromium and Nickel Cr_{eq} + Ni_{eq}, in accordance with the Schaeffler formula.

$$Q = 0.0102 \cdot \left(Ni_{eq} + Cr_{eq} \right) - 0.1144 \quad (2)$$

Third, the absence of macrodefects does not necessarily mean that the resulting weld strength is good enough. For that purpose, additional strength tests are required to ensure the welding is performing at least as good as the base materials. Besides, cyclic loadings can cause the appearance of such macrodefects, even later unleashing corrosion fatigue problems [33,34], and even permanent tensions can cause development of stress corrosion cracking if weld bead suddenly changes geometry or accelerates corrosion fatigue deterioration [35,36].

Nevertheless, regardless of such final strength, this study is still enough to demonstrate that a proper weld design, considering this strength, should be suitable for the whole service life, since the applied thermal input does not imply protective properties loss in the weld and HAZ zones.

Finally, as a last comment, following an analysis of the results on optimized thermal input obtained from the tests of the different coupons made of the three DSS in this study, it was concluded that DSS 2001 could not be welded with inputs as high as those for 2304 and 2205 steels, because the DSS 2001 material began to suffer perforations more easily than the other two as the input increased. Besides, evidence showed that 2205 DSS was also able to tolerate a slightly higher input than 2304 with no perforation. See Table 6.

Table 8. Thermal input to nickel and chromium equivalent content correlation.

Steel Grade	Ni_{eq}	Cr_{eq}	Ni_{eq} + Cr_{eq}	Q (KJ/mm)
2001	12	22,145	34,145	231
2304	134	261	395	293
2205	15	28	43	32

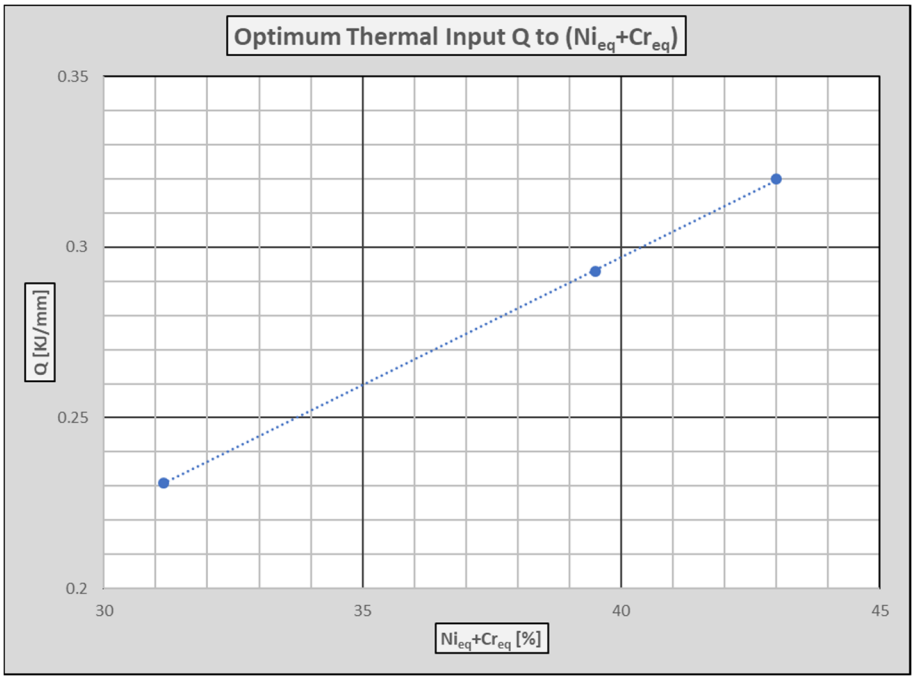

Figure 18. Optimum thermal input depending on equivalent Nickel and Chromium content.

5. Conclusions

1. Four types of Duplex Stainless Steel (DSS) joint samples, namely 2001 to 2001, 2304 to 2304, 2205 to 2205, and 2205 have been welded to carbon steel S275 for testing purposes. These DSS samples exceeded the maximum equivalent carbon rate for their theoretical classification as weldable steels in accordance with current structural standards [3–9], so an alternative procedure has been developed to ensure weldability.
2. Each DSS coupon sample has been welded holding certain boundary conditions constant, such as TIG welding without filler, no backing, no spacing, and no edge preparation, with automatic advance, and the same current intensity and voltage. Hence, the thermal input variation was simply controlled by varying only the welding speed. Several coupons of each material were therefore prepared with different thermal inputs.
3. Every coupon of the same DSS has been studied by means of non-destructive testing (NDT), according to the standard specifications for the certification of a welding procedure. Namely, visual inspection, radiographic X-ray tests and penetrating liquid tests. Those NDT were then

used to define the lowest optimum thermal input for welding an acceptable seam. Table 4 summarizes the optimum thermal input of each material.

4. Finally, to ensure remaining corrosion resistance to marine environments and chloride corrosion after welding, each specimen has been studied by means of a macrography to separate the base material, welding and heat-affected zones. Then several micrographies to obtain the ferrite content at each zone and detect indications of sigma, chi or other elements during a microstructural analysis, and finally a destructive accelerated corrosion test in a salt-spray chamber.
5. This study established a relationship between the heat generation during welding and the content of alloying elements in defect-free joints. Furthermore, it found that an increase in ferrite content did not lead to a worse corrosion resistance, as expected after passivation.
6. A salt spray test within a climatic chamber was performed on the different types of welded coupons according to EN ISO 9227 [22], using the Neutral Salt Spray (NSS) test, lasting up to 216 h, in order to demonstrate that the optimum thermal inputs had no effect on the corrosion resistance properties within the heat affected and welding zones. Following the application of the test, it was observed that the welded samples of DSS material 2001, 2304 and 2205 were corrosion free. In contrast, a continuous progression of red chloride corrosion was observed in the hybrid sample of combined materials 2205-S275, on the carbon steel half of the S275 coupon.
7. The results have shown suitable welding seams and an adequate weldability of the DSS materials 2001, 2304, and 2205 under the previously specified welding conditions, in terms of metallic continuity and corrosion behavior.
8. The hybrid welded joint of DSS steel 2205 and carbon steel S275 showed a bad performance under chloride environment as the carbon steel underwent appreciable corrosion, presumably when the joint became a galvanic couple, acting as a sacrificial anode.

Author Contributions: Conceptualization, I.C.-U.-A.; methodology, I.C.-U.-A.; formal analysis, E.B. and H.G.; investigation, A.M.; resources, I.C.-U.-A.; data curation, H.G. and E.B.; writing—original draft preparation, H.G. and E.B.; writing—review and editing, I.C.-U.-A.; visualization, A.M.; supervision, I.C.-U.-A. and A.M.; project administration, I.C.-U.-A.; funding acquisition, I.C.-U.-A. All authors have read and agreed to the published version of the manuscript.

Funding: This research was funded by ACERINOX EUROPA through Center for the Development of Industrial Technology (CDTI) within the frame of IISIS project, grant number IPT-20111023.

Acknowledgments: The tests presented in this manuscript were performed as part of the IISIS: "Investigación Integrada en Islas Sostenibles" (Integrated research in Sustainable Islands) research project, in receipt of funding from the Center for the Development of Industrial Technology (CDTI) and the Technological Fund, part of the Spanish Ministry of Industry, through the INNPRONTA research program. The final goal of the project is to research different technologies for building offshore island-cities, involving construction, energy and smart technologies with leading companies and research centers focused on each field. In the field of construction, the challenge is to develop modular construction and special marine reinforced concrete for the construction of islands that are capable of withstanding corrosive marine environments. In this context, most pathologies linked to reinforced concrete in marine environments are caused by rebar deterioration within the concrete and especially by chloride attack. The use of stainless steels is a very promising way to solve this problem, as has been demonstrated in several tests, among which those presented in this paper. Besides, the authors want to acknowledge Mario Oyarbide and Adrián Gastesi in particular for their technical support during the experimental campaign performed on these steels. Authors would like to acknowledge UPV/EHU PPGA19/61 contract as well as to the IT1314-19 (Basque Government) and GIU19/029 (UPV/EHU) research groups and to Laboratoire des ciencies de l'ingenieur appliquées, Fédération IPRA-EA4581, from the Université de Pau et Pays de l'Adour, for their support setting a cooperation framework. Finally, we are also especially thankful to ACERINOX EUROPA (part of the ACERINOX Group) for funding the IISIS project, supplying the necessary rebar samples for testing, and particularly to Rafael Sanchez and Julia Contreras from Technical Dpt./Labs for their expertise and for their commitment that greatly assisted our research.

Conflicts of Interest: The authors declare no conflict of interest.

References

1. Faccoli, M.; Roberti, R. Study of hot deformation behaviour of 2205 duplex stainless steel through hot tension tests. *J. Mater. Sci.* **2013**, *48*, 5196–5203. [CrossRef]

2. Saliba, N.; Gardner, L. Cross-section stability of lean duplex stainless steel welded I-sections. *J. Constr. Steel Res.* **2013**, *80*, 1–14. [CrossRef]
3. CEN. *Eurocode 2: Design of Concrete Structures—Part 1-1: General Rules and Rules for Buildings*; Comité Européen de Normalisation: Brussels, Belgium, 2004.
4. CEN. *Eurocode 3: Design of Steel Structures, Part 1-1: General Rules and Rules for Buildings*; Comité Européen de Normalisation: Brussels, Belgium, 2005.
5. CEN. *Eurocode 3: Design of Steel Structures, Part 1-4: General Rules-Supplementary Rules for Stainless Steels*; Comité Européen de Normalisation: Brussels, Belgium, 2006.
6. Espanya. *Código Técnico de la Edificación: (C.T.E.)*; Ministerio de Vivienda: Madrid, Spain, 2006; ISBN 978-84-340-1631-6.
7. Espanya. *Instrucción de Acero Estructural (EAE)*; Ministerio de la Presidencia: Madrid, Spain, 2011; ISBN 978-84-340-1980-5.
8. Espanya. *Instrucción de Hormigon Estructural. EHE-08*; Ministerio de Fomento: Madrid, Spain, 2011; ISBN 978-84-498-0899-9.
9. CEN. *Eurocode 3: Design of Steel Structures, Part 1-8: Design of Joints*; Comité Européen de Normalisation: Brussels, Belgium, 2005.
10. Verma, J.; Taiwade, R.V. Effect of welding processes and conditions on the microstructure, mechanical properties and corrosion resistance of duplex stainless steel weldments—A review. *J. Manuf. Process.* **2017**, *25*, 134–152. [CrossRef]
11. Paulraj, P.; Garg, R. Effect of intermetallic phases on corrosion behavior and mechanical properties of duplex stainless steel and super-duplex stainless steel. *Adv. Sci. Technol. Res. J.* **2015**, *9*, 87–105. [CrossRef]
12. Elsaady, M.A.; Khalifa, W.; Nabil, M.A.; El-Mahallawi, I.S. Effect of prolonged temperature exposure on pitting corrosion of duplex stainless steel weld joints. *Ain Shams Eng. J.* **2018**, *9*, 1407–1415. [CrossRef]
13. Vinoth Jebaraj, A.; Ajaykumar, L.; Deepak, C.R.; Aditya, K.V.V. Weldability, machinability and surfacing of commercial duplex stainless steel AISI2205 for marine applications—A recent review. *J. Adv. Res.* **2017**, *8*, 183–199. [CrossRef]
14. Kanemaru, S.; Sasaki, T.; Sato, T.; Mishima, H.; Tashiro, S.; Tanaka, M. Study for TIG–MIG hybrid welding process. *Weld. World* **2014**, *58*, 11–18. [CrossRef]
15. Kumar, M.L.S.; Verma, D.S.M.; RadhakrishnaPrasad, P. Experimental Investigation for Welding Aspects of AISI 304 & 316 by Taguchi Technique for the Process of TIG & MIG Welding. *Int. J. Eng. Trends Technol.* **2011**, *2*, 28–33.
16. Mohammed, G.R.; Ishak, M.; Aqida, S.N.; Abdulhadi, H.A. Effects of Heat Input on Microstructure, Corrosion and Mechanical Characteristics of Welded Austenitic and Duplex Stainless Steels: A Review. *Metals* **2017**, *7*, 39. [CrossRef]
17. M, M.A.; Shrikrishna, K.A.; Sathiya, P.; Goel, S. The impact of heat input on the strength, toughness, microhardness, microstructure and corrosion aspects of friction welded duplex stainless steel joints. *J. Manuf. Process.* **2015**, *18*, 92–106. [CrossRef]
18. Tasalloti, H.; Kah, P.; Martikainen, J. Effect of heat input on dissimilar welds of ultra high strength steel and duplex stainless steel: Microstructural and compositional analysis. *Mater. Charact.* **2017**, *123*, 29–41. [CrossRef]
19. Yang, Y.; Yan, B.; Li, J.; Wang, J. The effect of large heat input on the microstructure and corrosion behaviour of simulated heat affected zone in 2205 duplex stainless steel. *Corros. Sci.* **2011**, *53*, 3756–3763. [CrossRef]
20. Subramanian, G.; Palraj, S.; Balasubramanian, T.M. Galvanic corrosion interactions of zinc and SS.304 in the tropical marine atmosphere of Mandapam. *Anti-Corros. Methods Mater.* **1999**, *46*, 332–337. [CrossRef]
21. Paul, S.; Basu, K.; Mitra, P. A resistor-controlled sacrificial anode for cathodic protection of stainless steel in seawater. *Bull. Electrochem.* **2005**, *21*, 269–273.
22. ISO. *Corrosion Tests in Artificial Atmospheres—Salt Spray Tests*; International Standard Organization: Geneva, Switzerland, 2017.
23. Liu, X.; Xia, Z.; Zhou, H.; Yuan, B.; Li, Z.; Guo, F. Corrosion Behavior of Different Steel Substrates Coupled With Conductive Polymer under Different Serving Conditions. *J. Iron Steel Res. Int.* **2013**, *20*, 87–92. [CrossRef]
24. Yousefieh, M.; Shamanian, M.; Saatchi, A. Influence of Heat Input in Pulsed Current GTAW Process on Microstructure and Corrosion Resistance of Duplex Stainless Steel Welds. *J. Iron Steel Res. Int.* **2011**, *18*, 65–69. [CrossRef]

25. Sternhell, G.; Paul, D.; Taylor, D. Itzhak galvanic effects of various metallic couples on marine biofouling in a coral reef environment. *Corros. Rev.* **2002**, *20*, 453–468. [CrossRef]
26. Schaeffler, A.L. Constitution Diagram for Stainless Steel Weld Metal. *Met. Prog.* **1949**, *56*, 680.
27. ISO. *Non-Destructive Testing of Welds—Visual Testing of Fusion-Welded Joints*; International Standard Organization: Geneva, Switzerland, 2016.
28. CEN. *Non-Destructive Examination of Fusion Welds—Visual Examination*; Comité Européen de Normalisation: Brussels, Belgium, 1997.
29. CEN. *Non-Destructive Testing—Penetrant Testing—Part 1: General Principles*; Comité Européen de Normalisation: Brussels, Belgium, 1997.
30. CEN. *Non-Destructive Examination of Welds—Radiographic Examination of Welded Joints*; Comité Européen de Normalisation: Brussels, Belgium, 1997.
31. ISO. *Welding—Fusion-Welded Joints in Steel, Nickel, Titanium and Their Alloys (Beam Welding Excluded)—Quality Levels For Imperfections*; International Standard Organization: Geneva, Switzerland, 2014.
32. E04 Committee. *Test Method for Determining Volume Fraction by Systematic Manual Point Count*; ASTM International: West Conshohocken, PA, USA, 2019.
33. Calderon-Uriszar-Aldaca, I.; Briz, E.; Biezma, M.V.; Puente, I. A plain linear rule for fatigue analysis under natural loading considering the coupled fatigue and corrosion effect. *Int. J. Fatigue* **2019**, *122*, 141–151. [CrossRef]
34. Calderón-Urískar-Aldaca, I.; Briz, E.; Matanza, A.; Martin, U.; Bastidas, D.M. Corrosion Fatigue Numerical Model for Austenitic and Lean-Duplex Stainless-Steel Rebars Exposed to Marine Environments. *Metals* **2020**, *10*, 1217. [CrossRef]
35. Briz, E.; Martin, U.; Biezma, M.V.; Calderon-Uriszar-Aldaca, I.; Bastidas, D.M. Evaluation of the mechanical behavior of 2001 LDSS and 2205 DSS reinforcements exposed to simultaneous load and corrosion in chloride contained concrete pore solution. *J. Build. Eng.* **2020**, *31*, 101456. [CrossRef]
36. Calderón-Urískar-Aldaca, I.; Biezma, M.V.; Matanza, A.; Briz, E.; Bastidas, D.M. Second-order fatigue of intrinsic mean stress under random loadings. *Int. J. Fatigue* **2020**, *130*, 105257. [CrossRef]